Materials Science-Poland, *Vol. 26*, *No. 3*, *2008*

Structure and properties of the multilayers produced on Inconel 600 by the PACVD method with the participation of trimethylaluminum vapours*

R. SITEK[1**], K. SIKORSKI[1], J. SOBCZAK[2], T. WIERZCHOŃ[1]

[1]Faculty of Materials Science and Engineering, Warsaw University of Technology,
ul. Wołoska 141, 02-507 Warsaw, Poland

[2]Institute of Physical Chemistry, Polish Academy of Sciences,
ul. Kasprzaka 44/52, 01-224 Warsaw, Poland

The paper presents the results of examinations of the structure and properties of Al_2O_3 + Ni_3Al + Ni(Cr, Fe, Al) + Cr-Ni + Cr_7C_3 multilayers produced on nickel alloys by the plasma assisted chemical vapour deposition method with the participation of trimethylaluminum vapours in gaseous atmosphere. The layers have a high surface hardness of about 1200$HV_{0.05}$, and high heat and frictional wear resistance. In order to find a correlation between the structure of the multilayers and their properties, the following examinations have been executed: phase analysis by XRD and surface analysis by XPS, analysis of microstructure by optical and scanning electron microscopes as well as X-ray microanalyser, micro-hardness measurements, corrosion and frictional wear resistance testing.

Key words: *PACVD process; multilayers; Inconel 600; XPS*

1. Introduction

Creep-resistant austenitic nickel alloys belong to the group of materials widely used in industry for manufacturing turbine blades, sparking plug, compressor blades, exhaust reheater chambers, and nozzles of gas turbines, missile engines, and jet engines [1–5]. Owing to their high corrosion resistance, they find application in fabricating components of various chemical and petrochemical installations [5]. Heat-resistant nickel alloys can be exploited within the temperature range from 850 °C to 1250 °C [2]. As well known, the efficiency of an engine increases with temperature.

---

*The paper presented at the 9th Symposium on "Reactivity of Metastable Materials, 2007 EMRS Fall Meeting", Warsaw, 17–21 September, 2007.

**Corresponding author, e-mail: rsitek@inmat.pw.edu.pl

The temperature of gases in front of a turbine reaches the value of 1400 °C, thus, it should be lowered by cooling with air supplied partially from the compressor [3]. Another disadvantage of the nickel alloys is their poor resistance to frictional wear [6], which also restricts their application range. The materials alternative to the nickel super-alloys seem to be the intermetallic phases of the Ni–Al system which in the first place are lighter than the conventional nickel alloys and in addition show better resistance to oxidation and much better to frictional wear. A method of obviating the drawbacks of nickel super-alloys is to produce Ni–Al intermetallic layers on their surface using surface engineering techniques, which are highly economic and permit producing surface layers with a precisely specified chemical composition and the performance properties tailored to a given purpose [7].

In the present experiments Ni–Al intermetallic-based surface layers were obtained on Inconel 600 by subjecting the alloy to the plasma assisted chemical vapour deposition (PACVD) treatment with the participation of the trimethylaluminum metallorganic compound. In result of applying a thermo-chemical process, composite layers of σ-Al_2O_3 + Ni_3Al + Ni(Cr, Fe, Al) + Cr_7C_3 + Cr-Ni were obtained. The layers thus obtained show a good resistance to frictional wear and to corrosion. The properties of these layers chiefly depend on their phase compositions and the distribution of the individual phases between them.

2. Experimental

The chemical composition of the Inconel 600 samples used in the experiments is given in Table 1.

Table 1. Chemical composition of Inconel 600

Element	Mn	Cr	Fe	Si	Ti	Co	Al	Cu	C	Ni
Concentration [wt. %]	0.21	15.24	8.50	0.42	0.23	0.19	0.18	0.17	0.08	balance

The surface layers were produced on the Inconel 600 alloy using a glow discharge assisted PACVD process carried out in three stages realized in a single technological cycle, which was achieved by varying the chemical composition of the gaseous atmosphere and the process temperature. The initial stage was conducted at 400 °C with the atmosphere containing $Al(CH_3)_3$ vapours + hydrogen. The next stage, carried out at 550 °C, involved oxidation realized by introducing air (ca. 2 vol. %) into the reactive atmosphere. In the final stage, involving controlled diffusion processes, the treated samples were heated in an argon atmosphere at 850 °C. The phase composition of the obtained surface layer was analyzed in a Brucker D8 Discover diffractometer using CuK_α radiation in the 2θ range 20–100°, with the incidence angle of X rays, ω, ranging between 3° and 11°. The metallographic samples were prepared by cutting the

rods perpendicular to their surfaces, grinding with abrasive grades and finally polishing using polishing wheels and diamond pastes. Then the samples were etched with a reagent of the composition: 3g $FeCl_3$ + 10 cm^3 HCl + 90 cm^3 C_2H_5OH and observed under an Olympus IX70 optical microscope at the magnification of 1500×.

The chemical compositions of the surface layers were examined with a Cameca Semprobe SU-30 X-ray microanalyzer. The XPS spectra were recorded at various depths from the surface using a MICROLAB-350 (Thermo VG Scientific) spectrometer equipped with an X-ray radiation source. The analysis utilized the X-rays radiated by the Al Kα anode (1486.6 eV) operated at a power of 300 W (15 kV, 20 mA). The survey spectrum was recorded by scanning the energy range from 0 to 1350 eV at steps of 1 eV and pass energy of the spherical sector analyzer of 150 eV. The spectra of the individual C1s, O1s, Ti2p, N1s, Cr2p and Al2p regions were recorded at steps of 0.2 eV with the analyzer pass energy of 50 eV. The sample surface was bombarded with the Ar^+ ions supplied by an EX-05 ion gun and the spectra were recorded in function of the sputtering time proportional to the depth from the surface. The Ar^+ ions employed had energy of 3 keV and the magnitude of the ionic current was 1 μA. The spectra thus obtained were processed using the Avantage v.3.54 program (Thermo VG Scientific). The spectra were smoothed, the satellites due to the non-monochromatic radiation beam were removed, and the non-linear background was subtracted. The peaks were fitted using the shape of the synthetic peak constructed based on the Gauss and Lorentz shapes in a proportion of 70/30 (±5). Quantitative XPS analysis was executed on a layer surface before sputtering and on particular surfaces of layers after sputtering times of 10 335 s and 22 950 s. Fractures of the layers were examined by using a Hitachi S-3500N scanning electron microscope. The microhardness of the surface layers was measured by the Vickers method in a ZWICK Materialprüfung 3212002 hardness tester under the load of 50 G.

The examination of the corrosion resistance by the potentiodynamic method was performed in a NaCl + Na_2SO_4 solution (which simulated acidic rainfall of pH = 5.8) using a minicell installed on the sample surface. The cell was filled with an electrolyte, the rest potential (E_{ocp}) was determined and then the variation of the polarization current versus polarization potential was recorded and plotted. The polarization potential was varied from 300 mV (which was shifted towards the cathode potential by more than E_{ocp} value) to the anodic potential at the rate of 1 mV/s. All the potentials were referred to the potential of an Hg/HgO electrode. The intersection of the cathodic and anodic branches of the polarization curves indicated the magnitude of the corrosion current density $i_{corr.}$. The effect of the surface layers on the corrosion resistance of the material was evaluated based on the shift of the rest potential E_{ocp} determined for the modified surfaces with respect to the substrate potential, and also by calculating the protection degree using the formula (1).

$$\beta = \left(1 - \frac{i_{corr}^{w}}{i_{corr}^{p}}\right) \times 100\% \tag{1}$$

where: i_{corr}^{p} is the corrosion rate of the uncovered substrate, and i_{corr}^{w} is the corrosion rate observed in the material protected by the multi-component layer.

The frictional wear resistance of the layers was measured by the three rollers + taper method, and their adhesion to the substrate was examined using a Revetest device (CSEM Co). The loading rate was 100 N/min, the load ranged from 0 to 100 N, the sample feed rate was 10 mm/min and the acoustic emission sensitivity was 20.

3. Results

An X-ray phase and TEM [7, 8] analysis show that the layers produced by the PACVD method, carried out in a (H_2 + Ar) reactive atmosphere with the participation of the $Al(CH_3)_3$ metallorganic compound, are composite layers of the σ-Al_2O_3 + Ni_3Al + Ni(Cr,Fe,Al) + Cr_7C_3 + Cr-Ni type.

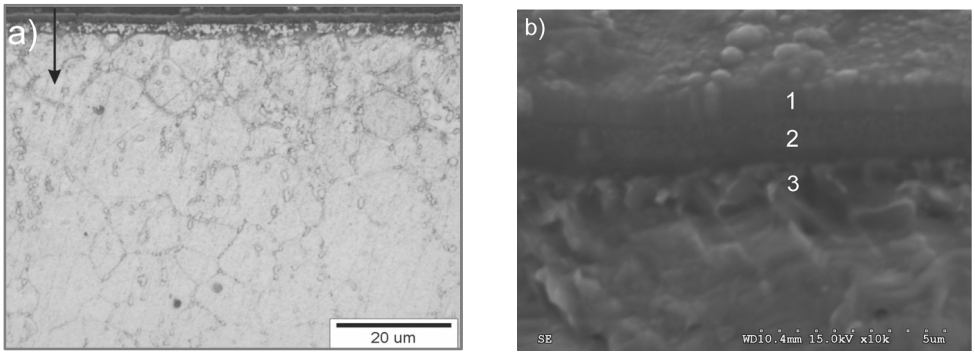

Fig. 1. Microstructure of a composite layer of the σ-Al_2O_3 + Ni_3Al + Ni(Cr, Fe, Al) + Cr_7C_3 + Cr-Ni type produced on the Inconel 600 by the PACVD method (a) and their fracture (b)

An image of the microstructure of the layer thus obtained is shown in Fig. 1a. The layer has a complex structure and is about 5 μm thick, which has been confirmed by the fractographic measurements (Fig. 1b). The layer appears to be composed of three zones.

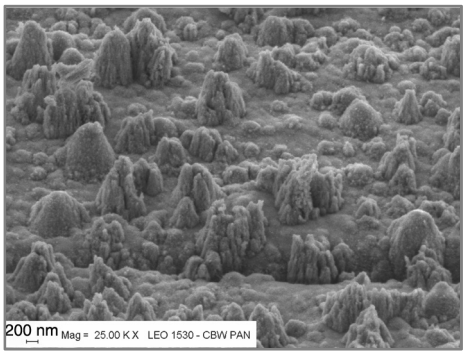

Fig. 2. Morphology of the surface of the σ-Al_2O_3 + Ni_3Al + Ni(Cr, Fe, Al) + $Cr0_7C_3$ 0+ Cr-Ni type layer produced by the PACVD method

The morphology of the surface of the layer is shown in Fig. 2. As can be seen, the layer has a finegrained structure. The fact that the grains are elongated suggests that the layer has grown in the columnar way. Its surface hardness is high, namely $1200HV_{0.05}$, which is indicative of an aluminum oxide film being present on the surface (the hardness of the substrate material is $220HV_{0.05}$).

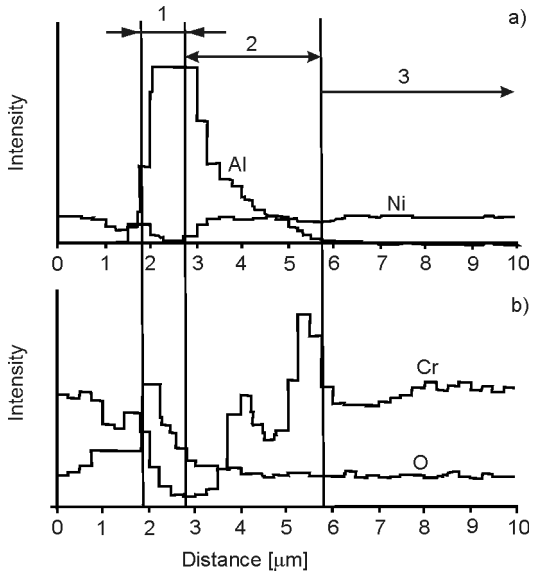

Fig. 3. Linear distribution of elements: a) Al and Ni, b) Cr and O on the cross-section of the composite layer; 1 – outer zone Al_2O_3, 2 – intermediate zone Al_2O_3 + Ni_3Al + Ni (Cr, Fe, Al), 3 – substrate Inconel 600

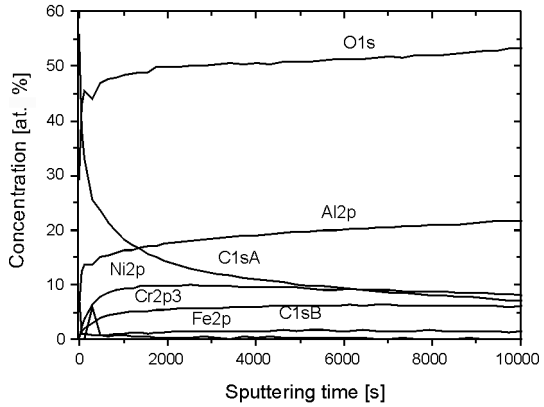

Fig. 4. Concentration profiles of elements in the outer layer (1) from the XPS analysis

Figure 3 shows the linear distribution of the elements identified on a cross-section of the sample obtained by X-ray microanalysis along the line shown in Fig. 1a. This distribution evidently shows that the layers are diffusively bound with the substrate (Fig. 3a). The increased concentration of chromium observed in the layer at a certain

depth (Fig. 3b) has already been explained by the formation of carbides in this zone [7, 8]. The outer zone of the aluminum oxide forms as a result of glow discharge assisted oxidizing (Fig. 3). Figure 4 shows the results of XPS examination of the outer zone of the layer. Detailed results of the analysis are given in Table 2.

Table 2. Concentration of elements *c* [at. %] and binding energies *E* of their compounds [eV] after ionic etching of various durations

Process	Ni $2p_{3/2}$		Fe $2p_{3/2}$		Cr $2p_{3/2}$		O1s		N1s		C1s		Al2p		Ti $2p_{3/2}$	
	E	*c*	*E*	*c*	*E*	*c*	*E*	*c*	*E*	*c*	*E*	*c*	*E*	at.%	*E*	*c*
Before etching	855.2	0.3	712.5	0.1	576.7	0.5	533.3	6.4	399.9	0.9	288.4	4.1	73.4	5.6	461.2	0.2
	852.9	0.2	710.8	0.4			531.8	17.1			286.3	9.9				
							530.3	8.9			284.6	44.9				
After 10 335 s Ar+	855.2	1.7	709.0	1.0	576.3	1.7	532.00	50.0	397.3	0.8	287.3	0.5	74.7	21.8	459.6	0.2
	852.9	7.5	707.0	2.3	574.3	2.8					285.9	1.6			456.6	0.1
											284.6	5.3				
											283.2	0.8				
After 22 950 s Ar+	854.9	0.7	711.4	1.3	577.6	0.8	532.29	52.6	397.6	1.0	288.39	0.2	74.9	25.3	462.0	0.1
	853.00	4.4	709.3	0.5	576.2	0.6					286.3	1.2				
			707.2	1.7	574.4	2.0					284.6	5.1				
											282.7	2.2				

Nickel present on the surface in trace amounts is much more visible at greater depths. Both on the surface and in the interior of the layer, it occurs in two basic states: as metallic nickel with binding energy of 852.92±0.1eV, and as NiO with its characteristic binding energy of 855±0.15 eV [9] (Fig. 5).

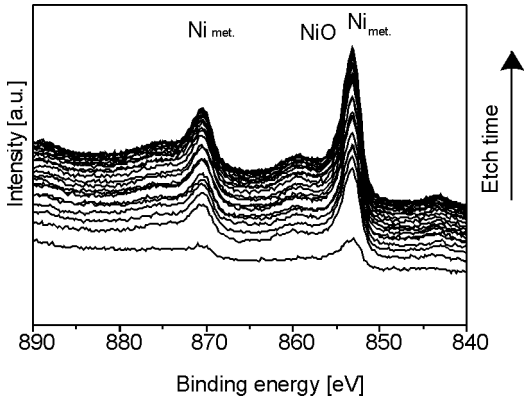

Fig. 5. XPS spectrum of the Ni2p region

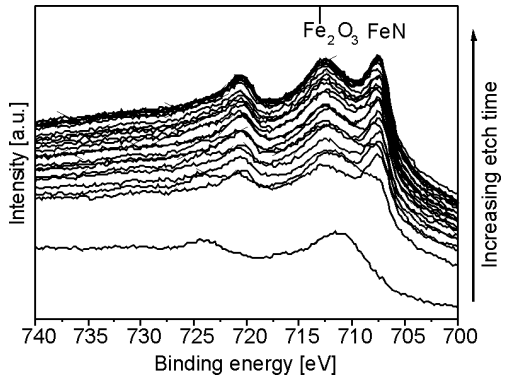

Fig. 6. XPS spectrum of the Fe2p3/2 region

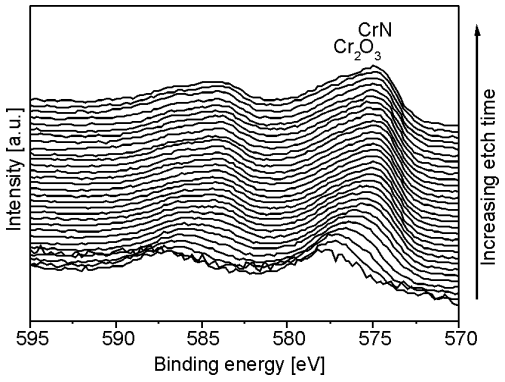

Fig. 7. XPS spectrum of the Cr2p region

Iron, occurring on the surface chiefly in the Fe_2O_3 form with binding energy of 710.8 eV, deeper in the layer also occurs in its metallic form with binding energy of about 707–708 eV (Fig. 6). Judging from the half-width of its peak, which in deeper zones of the layer is of the order of 2.4–2.6 eV, we cannot exclude that other iron compounds are also present, such as Fe-Ni with binding energy of 706.7 eV or Fe_3C with binding energy of 708.1 eV [10, 11]. Another broad peak visible in the Fe2p region corresponds to the binding energy of about 713 eV, which is above the value taken to be characteristic of the Fe_2O_3 type oxides, and should be ascribed rather to a satellite peak associated with the 'shake up' effect characteristic of the paramagnetic states of iron: Fe^{+2} and Fe^{+3} [9].

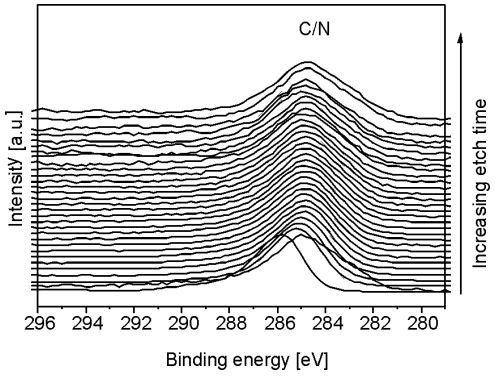

Fig. 8. XPS spectrum of the C1s region

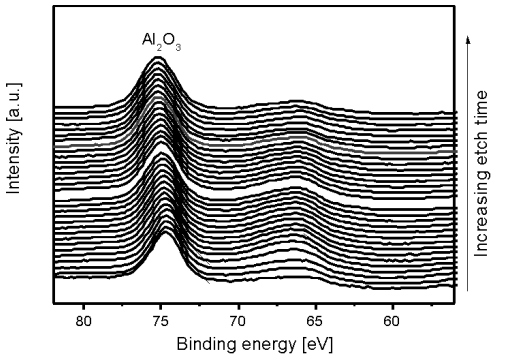

Fig. 9. XPS spectrum of the Al2p-Ni3p region

Chromium which, on the surface, occurs as the Cr^{3+} oxide with the binding energy of 576.6 eV [12], deeper in the layer is represented by a peak of the binding energy of about 575 eV (Fig. 7). A precise identification of this peak by XPS is not possible, since the peaks ascribed to the Cr-N bonds and the peaks due to the Cr-C bonds overlap one another [13–17]. The presence of carbides is confirmed by the clear broadening of the carbon peak towards lower energies, which can be seen in Fig. 8 in deeper

regions of the layer, and in the results of the TEM analysis described in [7, 8]. The only element which does not change its state in deeper zones of the layer is aluminum with binding energy of the Al2p peak equal to about 74.7 eV which is characteristic of the Al_2O_3 phase (Fig. 9).

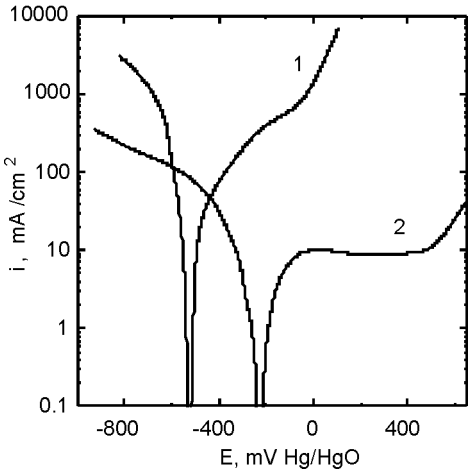

Fig. 10. Anodic polarization curves obtained for : 1 – untreated, 2 – PACVD-treated Inconel 600 immersed in an NaCl + Na_2SO_4 solution (simulating acidic rainfalls with pH = 5.8)

Table 3. Results of corrosion examinations

Material	E_{ocp} mV, Hg/HgO	$E_{corr.}$ mV, Hg/HgO	i_{corr} μA/cm^2	$i_{passive}$ μA/cm^2	Anticorrosion protection degree, β %
Inconel 600 (substrate)	–170	–460	1,5	–	–
Inconel 600 covered with the multilayer	–50	–240	<0,1	10	99

Corrosion examinations (Fig. 10, Table 3) performed in a NaCl + Na_2SO_4 solution (which simulated acidic rainfall of pH = 5.8) using the potentiodynamic method have shown that the σ-Al_2O_3 + Ni_3Al + Ni(Cr, Fe, Al) + Cr_7C_3 + Cr-Ni type composite layer formed on the Inconel 600 alloy improves the corrosion resistance of the alloy. This can be inferred from the facts that, in the alloy with the surface composite layer, the open circuit potential (E_{ocp}) and the corrosion potential ($E_{corr.}$) are shifted more towards the anodic potential and the corrosion current density $i_{corr.}$ is considerably lower (at $i_{corr.}$=10 μA, the anodic curve shows the passive state). The very high degree of anti-corrosive protection ensured by the composite layer is achieved thanks to its tightness (no cracks developed through the layer to the substrate).

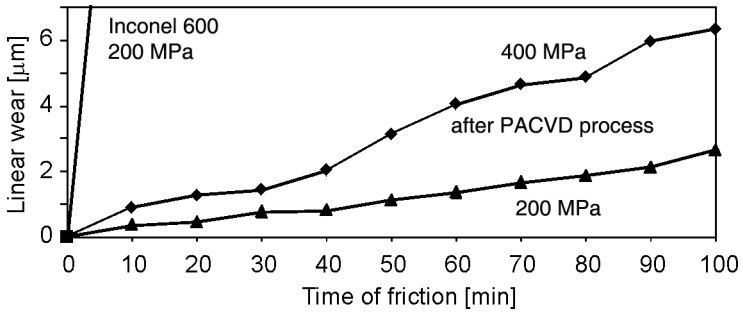

Fig. 11. Linear wear of an σ-Al_2O_3 + Ni_3Al + Ni(Cr, Fe, Al) + Cr_7C_3 + Cr-Ni type composite layer in function of friction time compared to the wear observed in the Inconel 600 alloy

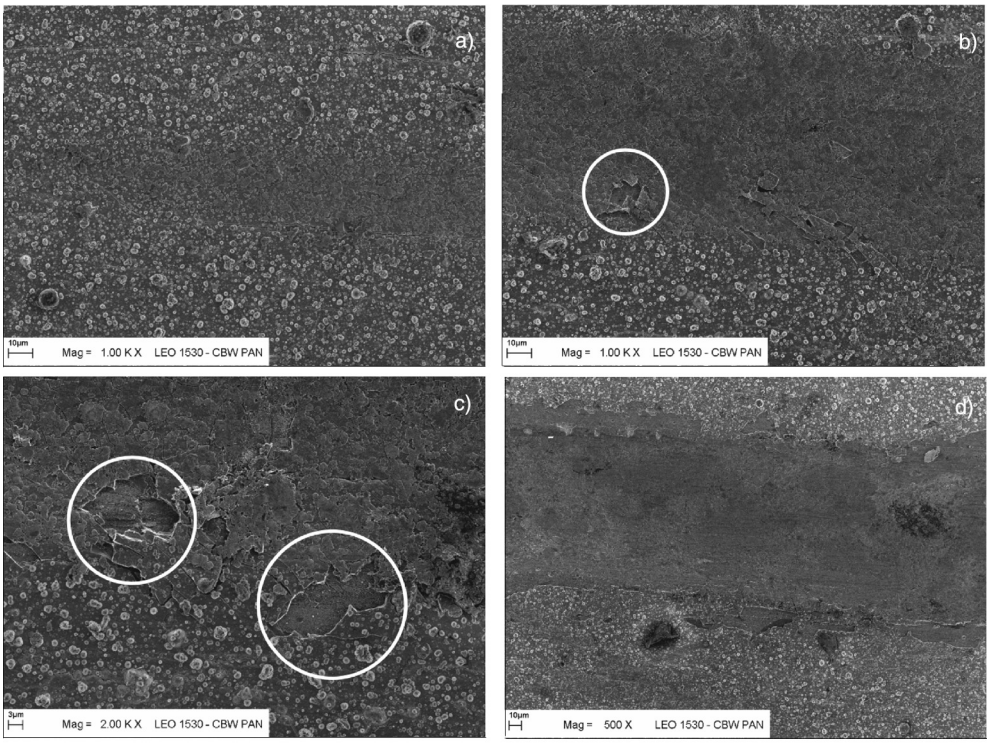

Fig. 12. Surface of an σ-Al_2O_3 + Ni_3Al + Ni(Cr, Fe, Al) + Cr_7C_3 + Cr-Ni type composite layer after the scratch test: a) initial stage of the test, b) *Lc* = 3.57 N, indenter cutting path 0.35 mm, c) *Lc* = 7.27 N, indenter cutting path 0.7 mm, d) *Lc* = 42.96 N, indenter cutting path 0.5 mm

The presence of the Al_2O_3 surface zone and of sublayers composed of Ni-Al intermetallic phases greatly improves the frictional wear resistance of Inconel 600 (Fig. 11). Untreated Inconel 600 examined under the load of 200 MPa is seized as early as after 10 min of the test, whereas the alloy covered with the multi-component

composite layer does not undergo seizure during the entire friction test, i.e. 100 min, even when higher loads of 200 and 400 MPa are applied. The results of the scratch test (Fig. 12) have shown that despite its complex structure, the layer adheres well to the substrate, which is an important performance property. At the initial stage of the indenter penetration, we can only see abrasion (Fig. 12a). The first single splinters are observed at the critical force Lc = 3.57 N at an indenter cutting path of 0.35 mm (Fig. 12b). Numerous splinters occur at Lc = 7.27 N after the indenter runs a cutting path of 0.7 mm (Fig. 12c), and finally the break-through of the ayer is observed at Lc = 42.96 N after a cutting path of 5 mm (Fig. 12d). It should however be noted that the layers are relatively thin with the thickness of the outer Al_2O_3 ceramic zone not exceeding 1 μm. Moreover, although the ceramic is very hard and resistant to compression, its tensile strength is not very high.

4. Conclusions

When applied to an Inconel 600 substrate, the PACVD process carried out with the participation of the $Al(CH_3)_3$ metallorganic compound yields a multi-component composite layer of the σ-Al_2O_3 + Ni_3Al + Ni(Cr,Fe,Al) + Cr_7C_3 + Cr-Ni type during a single technological cycle. The layer can be produced on Inconel 600 alloy parts with complicated shapes.

The layers thus obtained have a high hardness, due to the outer Al_2O_3 ceramic zone which also ensures their enhanced corrosion resistance,

The diffusion character of the individual sub-layers guarantees their good adherence to the Inconel 600 substrate and improve the tribological and mechanical properties.

Acknowledgement

Surface characterizations were performed using a Microlab 350 located at the Physical Chemistry of Materials Center of the Institute of Physical Chemistry, Polish Academy of Sciences and of the Faculty of Materials Science and Engineering at Warsaw University of Technology.

References

[1] KENNEDY L.R., THOMAS M., Adv. Mater. Processes, 149 (1996), 33.
[2] MIKUŁOWSKI B., Stopy żaroodporne i żarowytrzymałe, Wydawnictwa AGH, Kraków 1997.
[3] GODZIMIRSKI J., Technika i Eksploatacja, 5 (2006), 52 (in Polish).
[4] EZUGWU O.E., Int. J. Machine Tools Manuf., 45 (2005), 1353.
[5] DOBRZAŃSKI L., Podstawy nauki o materiałach i metaloznawstwo, WNT, Gliwice Warszawa 2002.
[6] DONG-GOO KIM, YOUNG-ZE LEE., Wear, 250 (2001), 673.
[7] TACIKOWSKI M., SŁOMA J., WOŹNIAK M., WIERZCHOŃ T., Intermetallics, 14 (2006), 123.
[8] TACIKOWSKI M., SITEK R., SIKORSKI K., WIERZCHOŃ T. (in critical review in Intermetallics).
[9] NIST X-ray Photoelectron Spectroscopy Database 20, Version 3.4, http://srdata.nist.gov/xps/.
[10] GONTIJO L.C., MACHADO R., MIOLA E.J., CASTELETTI L.C., NASCENTE, Surf. Coatings Technol., 183 (2004), 10.

[11] BONNET F., ROPITAL F., LECOUR P., ESPINAT D., HUIBAN Y., GENGEMBRE L., BERTHIER Y., MARCUS P., Surf. Interf. Analysis, 34 (2002), 418.
[12] GROHMANN I., KEMNITZ E., LIPPITZ A., Surf. Interf. Analysis, 23 (1995) 887.
[13] DETROYE M., RENIERS F., BESS-HERMAN C., VAREECKEN J., Appl. Surf. Sci., 144–145 (1999), 78.
[14] GROUDEVA-ZOTOVA S., VITCHEV R.G., Surf. Interf. Analysis, 30 (2000), 544.
[15] LIPPITZ A., HÜBERT TH., Surf. Coatings Technol., 200 (2005) 250.
[16] FIGUEROA C.A., ALVAREZ F., J. Appl. Phys., 97 (2005), 103528.
[17] RIVERE J.P., CAHOREAU M., MEHEUST P., J. Appl. Phys., 91 (2002), 6361.

Received 25 February 2008